Fragmentation dynamics of molecular hydrogen in strong ultrashort laser pulses

A. Rudenko, B. Feuerstein, K. Zrost, V.L.B. de Jesus*, T. Ergler,
C.D. Schröter, R. Moshammer, and J. Ullrich
Max-Planck-Institut für Kernphysik, D-69029 Heidelberg, Germany

* present address: Centro Federal de Educação Tecnológica de Química de Nilópolis/RJ,
Rua Lucio Tavares 1045, Centro - Nilópolis - 26530-060, Rio de Janeiro, Brazil

We present the results of a systematic experimental study of dissociation and Coulomb explosion of molecular hydrogen induced by intense ultrashort (7-25 fs) laser pulses. Using coincident recoil-ion momentum spectroscopy we can distinguish the contributions from dissociation and double ionization even if they result in the same kinetic energies of the fragments. The dynamics of all fragmentation channels drastically depends on the pulse duration and for 7 fs pulses becomes extremely sensitive to the pulse shape.

32.80.Rm, 31.90.+s, 32.80.Fb

1. Introduction

The fragmentation and ionization of the two simplest molecules H_2 and H_2^+ (or alternatively D_2/D_2^+) in intense optical fields has been extensively studied both theoretically and experimentally. In contrast to the atomic case, the molecule exhibits three timescales, the fast electronic motion (as scale), the vibrational (fs scale) and rotational (ps scale) nuclear motion. The vibrational degree of freedom is of particular interest since its timescale matches the duration of state-of-the-art optical laser pulses.

Considerable theoretical work was done for the neutral hydrogen molecule (see, e.g. Yu *et al* 1996, Walsh *et al* 1998, Harumiya *et al* 2002, Saenz 2002a,b) and for the molecular ion (see, e.g. Zuo and Bandrauk 1995, Chelkovski *et al* 1996,1999, Numico *et al* 1997, Dundas *et al* 2000, Bandrauk and Shon 2002, Feuerstein and Thumm 2003). Some specific properties make the latter a model laboratory system for laser-matter interactions. First, there exists only one bound potential curve, i.e. the electronic ground state - all other electronically excited states are purely repulsive and converge towards the Coulombic $1/R$ curve, where R is the internuclear distance (see Figure 1). Second, the degeneracy of the two lowest electronic states $1s\sigma_g$ and $2p\sigma_u$ lead to a strong dipole interaction of these levels in the presence of external electrical fields which is essential for the coupling of the system to laser radiation. Third, the quite large difference in the ionization energies of H_2 (15.2 eV) and H_2^+ (29.9 eV) is the basis of a two-step treatment: Starting with the neutral molecule in a strong laser pulse the first electron will be easily removed creating the ionic state which will subsequently undergo further fragmentation processes. Most experiments have used the neutral molecule as a target (Zavriyev *et al* 1993, Walsh *et al* 1997, Thomson *et al* 1997, Gibson *et al* 1997, Frasinski *et al* 1999, Posthumus *et a*l 2000, Rottke *et al* 2002). However, the formation and fragmentation of H_2^+ occurs in the same laser pulse and, thus, cannot be completely disentangled (Walsh *et al* 1998).

Hence, there is a growing interest in using molecular ions as targets (Williams *et al* 2000, Sändig *et al* 2000, Shellhammer *et al* 2000) or in getting better insight into the time dependence of the fragmentation dynamics. The latter is not at last stimulated by the fact that in contrast to the ionic case using a neutral molecule as a target opens an additional possibility to probe the dynamics of the nuclar motion. Recently the pioneering concept of a "molecular clock" (Niikura *et al* 2002,2003, Alnaser *et al*

2003) was introduced. The idea is based on the so-called recollision model (Corkum 1993). Here, one considers the combined propagation of the nuclear and electronic wavepackets, which is started by the first ionization step. The emitted electron is driven back and forth by the oscillating laser field and may recollide after a well-defined time with its parent ion while the nuclei have moved apart according to their motion on the new H_2^+ potential curve. Emission of the second electron induced by the recollision leads to Coulomb explosion (CE) of the molecule, which provides a mapping of the nuclear wavepacket at the time of recollision via the relation of the kinetic energy release (KER) of the fragments $E_{kin} = 1/R$. However, to read the "molecular clock" one has to know via which channel the fragmentation takes place. This requires a detailed and comprehensive modelling of the recollision process. Very recently, good agreement of theory and experiment has been achieved (Alnaser *et al* 2003, Tong *et al* 2003). However, there are still open questions remaining. In particular, there is an ongoing debate whether recollision-induced dissociation contributes to the fragments detected in the “molecular clock” scheme.

The present work focuses on the influence of the temporal structure of short and ultrashort (< 10 fs) laser pulses on the fragmentation dynamics of H_2 and on the problem of reliable distinguishing between the contributions from the dissociation and CE for the cases where they lead to fragments with similar kinetic energies. The paper is structured as follows: In Section 2 a brief description of the experimental set-up is given, followed by an overview of the various fragmentation channels and the driving mechanisms in section 3. The experimental results are presented and discussed in Section 4, and conclusions are given in Section 5.

2. Experimental setup

The measurements were performed using a new "reaction microscope" (Ullrich *et al* 2003) designed to meet the specific requirement of the experiments with high-intensity lasers (see de Jesus *et al* 2004a for details). We used linearly polarized radiation of a Kerr-lens mode locked Ti:sapphire laser at 795 nm wavelength with 25 fs pulse width (FWHM). To generate few-cycle pulses they were spectrally broadened in a gas-filled hollow fiber and then compressed to 7 fs (FWHM) by chirped mirrors and a prism compressor. Fluctuations of the laser intensity from pulse to pulse were monitored during the experiment and did not exceed 5%. Absolute calibration of the peak intensity was performed using a clear kink in the measured photoelectron momentum distribution, which corresponds to the maximum drift momentum of $2\sqrt{U_p}$ that electrons can gain from the laser field (de Jesus *et al* 2004b).

The laser beam was focused to a spot size of ~ 7 μm on the collimated supersonic gas jet in the ultra-high vacuum chamber ($2\cdot10^{-11}$ mbar). Charged reaction fragments were guided to two position-sensitive channel plate detectors by weak electric (2 V/cm) and magnetic (7 G) fields applied along the laser polarization axis. From the time-of-flight and position on the detectors the full momentum vectors of the recoil ions and electrons were calculated.

A typical time-of-flight (TOF) spectrum of H_2 fragmentation by 25 fs laser pulse is shown in Figure 2a. The most prominent line at the right side of the spectrum corresponds to H_2^+ ions. H^+ fragments form two groups of peaks nearly mirror symmetric with respect to the full vertical line indicating the TOF of the protons with zero longitudinal (along the polarization direction) momentum. 'Forward' protons are those going directly to the ion detector, while 'backward' ones go first to the opposite hemisphere and then are turned back by the extraction field. Thus, the H^+ peaks

corresponding to the various fragmentation channels appear twofold in the spectrum. Slight asymmetry in the peaks position is due to the fact that the longitudinal momentum is not exactly linear with TOF. Here it should be noted that the heights of the peaks, i.e. the branching ratios of the different channels depend on the acceptance of the spectrometer, which differs for different fragment energies (see de Jesus et al 2004a for details). Thus only the qualitative changes of these ratios with intensity and pulse duration will be considered here.

Figure 2b shows corresponding energy spectrum for the 'forward' protons, where the same set of peaks can be seen. Fragmentation mechanisms giving rise to these structures are discussed in the next section.

3. Fragmentation channels of H_2 in strong 800 nm laser pulses

Figure 1 shows the different ionization and fragmentation pathways of H_2 in a strong 800 nm laser field in form of a potential curve diagram. By single ionization of H_2 the initial vibrational ground state is promoted in a vertical transition onto the electronic ground state potential curve $1s\sigma_g$ of H_2^+. Since the wave packet is not an eigenstate anymore it will start to propagate on the new potential curve defining a timescale for subsequent fragmentation processes. The molecular ion can either dissociate or be further ionized leading to a pair of protons (Coulomb explosion). Up to now there were no experimental evidences found for direct molecular dissociation leading to a pair of neutral hydrogen atoms (Posthumus 2004).

2.1 Dissociation

Dissociation is driven by a strong dipole interaction of the two lowest electronic states $1s\sigma_g$ and $2p\sigma_u$ in the presence of a strong field along the molecular axis. In a cycle-

averaged Floquet description (Shirley 1965, Bandrauk and Sink 1981) one finds a series of dressed potential curves spaced by the photon energy. Via avoided crossings the molecular ion can dissociate by a net absorption of one or two photons. In the latter case, absorption of three photons in the first avoided crossing is followed by a re-emission of one photon at the second crossing. Since for each photon the parity of the molecular state must change, there is no direct two-photon process. In the fragment kinetic energy spectrum (see Figure 2b) these channels manifest themselves as two peaks below 1 eV per proton (1ω and 2ω peaks). A comprehensive discussion on the dynamics and interplay of different dissociation mechanisms referred to as "bond softening" (Bucksbaum *et al* 1990), vibrational trapping, or "bond-hardening" (Frasinsky *et al* 1999), "above-threshold" (Giusti-Suzor *et al* 1990),"below-threshold" (Numico *et al* 1997) or "zero-photon" (Posthumus *et al* 2000) dissociation can be found in the reviews of Giusti-Suzor *et al* (1995) and Posthumus (2004).

2.2 Sequential double ionisation (SDI)

The mechanism of SDI in strong laser fields, which is well known for atoms, becomes more complex in the molecular case since the ionisation potential of the molecular ion depends on the internuclear separation *R*. In addition, at intermediate *R* an even stronger enhancement of the field ionisation rates is observed due to the interaction of the $1s\sigma_g$ and $2p\sigma_u$ states, which causes an oscillating localisation of the electron cloud at one of the nuclei. This effect of charge resonance enhanced ionisation (CREI) gives the largest ionisation probabilities for H_2 in a range of internuclear distance from 3.5 to 7 a.u. corresponding to a KER per proton of 2 to 4 eV (Figure 2b). Since the dipole interaction occurs along the molecular axis, the corresponding CE contribution is strongly peaked along the laser polarization direction (Posthumus 2004). CREI was

found to be a dominant SDI channel in most of the measurements on H_2 and D_2. However, the results of recent experiments (Legare *et al*. 2003, Osipov *et al* 2004) have shown that if few-cycle laser pulses are used, the “atomic-like” SDI, which results in more energetic CE fragments with more isotropic angular distribution, starts to compete with CREI. In (Legare *et al*. 2003) these two channels were referred to as “sequential ionization” and “enhanced ionization”. This should not lead to confusion: both processes are definitely sequential and the essential difference is the extreme R–dependence of the “enhanced ionization” (CREI).

2.3 Non-sequential double ionisation (NSDI)

In the case of a linearly polarized laser field the first emitted electron can be driven back and recollide after about three quarters of an optical cycle with its parent ion. The returning electron may either kick out directly the second electron through recollision-ionization (RI) or promote the bound electron into an excited state, which can then be easily field ionised. This mechanism of recollision-excitation followed by subsequent field ionisation (RESI) was found to play a decisive role for NSDI of atoms (Feuerstein *et al* 2001, de Jesus *et al* 2004a,b). For H_2 the NSDI channel has been identified as a high-energy shoulder in the fragment energy spectra for linear polarization, which disappears in the circular case as shown in Figure 2b (see also Staudte *et al* 2002, Sakai *et al* 2003, Legare *et al* 2003). NSDI leads to the largest fragment energies since it is a fast process, which for the first electron return gives the nuclei less than one optical cycle to separate. In a recent work based on the "molecular clock" principle mentioned above it was shown by comparison of experimental and theoretical results that RESI is the dominating NSDI channel (Alnaser *et al* 2003, Tong *et al* 2003).

4. Results and discussion

4.1 From short to ultrashort pulses: Influence of the pulse shape

Figure 3 shows the evolution of the time-of-flight (TOF) spectra of the H_2 fragments with the decreasing pulse duration. The spectra for 25 fs pulses at peak intensities of 0.2, 0.3 and 0.5 PW/cm^2 are shown in figure 3a. Similar to Figure 2a, with lowest kinetic energy we find the 1ω and 2ω dissociation peaks followed by the broad structure due to CREI. As the intensity is increased the branching ratio of the 1ω vs. 2ω dissociation becomes smaller and CE starts to compete with the dissociation channel. A similar intensity dependence of the spectra was observed in previous experiments (Thomson *et al* 1997, Staudte *et al* 2002). If we now reduce the pulse duration while keeping the peak intensity approximately fixed the fragmentation pattern changes significantly (Figure 3b: 10 fs, Figure 3c: 7 fs). We find the branching ratio of 1ω and 2ω dissociation channels reversed and the corresponding peaks broadened, a feature that will be discussed in section 4.3. With the decreasing pulse duration we observe a strong suppression of the CE (CREI) channel compared to dissociation. Intuitively it is apprehensible: when the pulse length becomes shorter than the vibrational period, the pulse may be gone before the molecule extends to the critical internuclear distances corresponding to the region of enhanced ionization.

Figure 3c depicts two spectra obtained with the pulses of the same temporal width (FWHM) (7 fs) but different shapes. Figure 4 shows the measured frequency spectra (, the Fourier limit for the intensity profile and measured 2nd order autocorrelation for both pulses. Autocorrelation patterns calculated from the spectra are very close to the measured ones. Panels (a)-(c) and (d)-(f) in Figure 4 correspond to the curves 1 and 2 in Figure 3c, respectively. For the curve 1, similar to the results of Legare *et al* (2003)

on D_2, we find a splitting of the CE peak into two components, one corresponding to CREI, and one with higher energies, whereas for the curve 2 only the outer peak can be observed. In order to elucidate this effect in more detail, we consider the correlated longitudinal (along the field polarisation direction) momenta of two protons detected in coincidence as shown in two-dimensional diagrams in Figure 5 for 25 fs (a) and 7 fs (b) pulse width, respectively. The true coincidences are found close to the diagonal reflecting almost zero sum momentum. The remaining width is due to the momentum defect carried away by the electron which is not shown here (see de Jesus *et al* 2004a). All other events are due to random coincidences, mainly with protons from dissociation as it can be seen from the projected momentum spectra on the top and on the left side. In Figure 5a CREI events are found in the broad maximum on this diagonal whereas the events due to recollision form the tail extending to larger momenta. The small peak around ±9 a.u. consists mainly of false events due to the crossing of two bands of random coincidences. The correlation diagram for the 7 fs pulse, which belongs to the curve 1 of Figure 3c, reveals again the disappearance of the broad CREI peak and, instead, two new peaks in its flanking parts. At lower momenta (±14 a.u.) a third peak shows up, which is certainly not an artefact since it does not fit to a band of random coincidences. Assuming all proton energy to be due to the Coulomb explosion the internuclear distance R at the time when the second electron was removed can be extracted from the peak positions. Here, we find R = 3.2 a.u. and R = 5.7 a.u. for the two peaks visible in Figure 3c. The third peak corresponds to R = 9.4 a.u. and, hence, the question arises how the nuclear wave packet can reach that distance within the duration of the pulse. This leads us back to Figure 3c and the dependence on the pulse shape.

As it can be seen from Figure 4, for those cases where we find in the correlation spectrum a clear splitting of SDI peak the pulse shape was affected by quite strong pre and post pulses. By optimizing the pulse shape, i.e. suppressing the pre and post pulses (Figure 4d–f) two low-energy peaks are suppressed and only the peak with the highest kinetic energy (and consequently shortest delay between removal of the first and second electron) survives (curve 2 in Figure 3c). This proves that the pre and post pulses were strong enough for a subsequent ionization on a time scale of 15 to 25 fs which is much longer than the FWHM of the main peak of the temporal pulse profile. This critical dependence on the pulse shape is due to the from the fact that the molecular ion becomes more and more sensitive to field ionization as it expands with time and reaches the region of enhanced ionization where even a weak post pulse can remove the second electron. From a more technical point of view, this behaviour makes H_2 a sensitive probe for the quality of ultrashort laser pulses which could be used as a diagnostic tool.

4.2 Sequential double ionization

The intensity dependence of the proton energy spectra for ultrashort pulses with a "clean" temporal profile, i.e. without significant pre and post pulses, is depicted in Figure 6. Here only the most energetic SDI peak, where the second ionization step occurs before the internuclear distance reaches the region of enhanced ionization, can be resolved. However, some residual structures on the position of two low-energy double ionization peaks still can be observed in the coincidence diagrams. This is more pronounced for the highest intensities: indeed, for a peak intensity of PW/cm^2 the post pulses on a level as low as 1% can still result in a considerable amount of enhanced ionization events.

Over the peak intensity range from 0.2 to 2.0 PW/cm^2 SDI starts from almost negligible contribution at the lowest power density and becomes finally comparable with the dissociation channel. The maximum of the SDI peak shifts from 4.1 eV for 0.2 PW/cm^2 to 5.2 eV for 2.0 PW/cm^2 which corresponds to an internuclear separation of R = 3.3 a.u. and R = 2.6 a.u., respectively. This effect has been recently demonstrated theoretically by Tong and Lin (2004). In their simulations for D_2 the peak positions of ~ 6.2 eV at 3.2 PW/cm^2 and ~ 5.7 eV at 2.4 PW/cm^2 are predicted, which is in good qualitative agreement with our results. This shift is due to the fact that for the same pulse duration at higher peak intensities the second ionization step can occur earlier, at smaller values of R and thus resulting in larger Coulomb energies of the fragments. The effect is less pronounced in the low intensity regime, most likely due to a stronger R-dependence of the ionization probability (Plummer and McCann 1996). A similar shift is observed for the CREI peak (Figure 3a, see also Walsh *et al* 1997).

4.3 Recollision-induced double ionization

For NSDI of atoms by strong linearly polarized fields the electron correlation is partly reflected by the sum momentum of the electrons parallel to the laser polarization direction. In the case of an atom this is identical to the negative recoil momentum of the doubly charged ion. It is known that the ion momentum distributions along the field polarization direction for NSDI are significantly broader than for SDI (Weber *et al* 2000). It can even exhibit clear maxima at nonzero momenta ("double-hump" structure) in the case of a dominance of RI as, e.g. for Ne (de Jesus *et al* 2004b). If RESI is the dominating mechanism of NSDI one finds a maximum at zero momentum but still a broader distribution compared to SDI (Feuerstein *et al* 2001). In the case of

H_2 one has to consider the sum (or centre-of-mass) momentum of the two protons which plays the role of the recoil ion momentum in the atomic case and balances the sum momentum of the electrons. Figure 7 shows the protons sum momentum distributions for the CREI and NSDI channels for 25 fs and 7 fs laser pulses. In both cases one finds a significantly broader distribution for NSDI compared to CREI. A double-hump structure is not found in the recollision case providing additional evidence that RESI is the dominating mechanism as it has been recently discussed by Tong *et al* (2003). It can be noticed that the NSDI momentum distribution is slightly broadened for a few-cycle pulse while the SDI spectra have almost the same widths. Low statistics does not allow us to draw a conclusion whether this broadening indeed reflects some changes in the recollision dynamics. To clarify this point, kinematically complete experiments on rescattering-double ionization of H_2 are under way.

4.3 Dissociation in ultrashort pulses

When the laser pulse duration is decreased from 25 to 10 fs, the most remarkable change in the low-energy part of the proton spectrum is the reversed branching ratio of 1ω and 2ω dissociation channels (Figure 3a and 3b). Enhancement of the 1ω peak for tpulses with very short rise-times was discussed by Nomico *et al* (1997) in terms of “below-threshold” dissociation. Later, Frasinski *et al* (1999) experimentally observed the dynamical shift of this structure to higher energies with decreasing pulse duration, which was associated with the different speed of the release of the trapped wave packet at the falling edge of the pulse. For 10 and 7 fs pulses we also observe a slight shift of the position of the 1ω peak compared to 25 fs. However, it is not clear to which extent effects like vibrational trapping or “below-threshold” dissociation can contribute in our case of high intensities. In general, with decreasing temporal width

of the pulse the shape of the dissociation part of the spectrum deviates more and more from the two-peak structure corresponding to the 1ω and 2ω dissociation channels (see curve 2 in Figure 3c). The reason for this, apart from the broadening of the photon spectrum, is the breakdown of the Floquet model for the dissociation which assumes a quasi-CW laser field. The propagation of the wavepackets on the light-induced potential curves via avoided crossings (see Figure 1) into the dissociation continuum needs time. If the pulse duration becomes shorter than the time required to reach the level crossings, this mechanism does not work anymore, similar to the suppression of CREI discussed above. However, even in the limit of an infinitely short "δ-like" pulse the molecule will still have a finite probability to dissociate, since the vertical (Franck-Condon) transition from H_2 to H_2^+ in the preceding single ionization gives rise to a small overlap of the initial nuclear wave function with the dissociation continuum of H_2^+. The corresponding fragment energy distribution is compared to the experimental result for a 7 fs pulse in Figure 6. The best agreement is found for 0.8 PW/cm^2 with a residual deviation most likely due to the finite pulse duration. This difference becomes stonger stronger at higher intensities in form of a partial reappearance of the two light-induced dissociation peaks since even weak post pulses may be strong enough to open the dissociation paths through the avoided crossings. (This can be confirmed by comparison of the curves 1 and 2 in Figure 3c). The lower intensity shows a remarkable lack of higher dissociation energies compared to the Franck-Condon distribution. This is most likely caused by the *R*-dependent ionization potential of H_2 which leads to a strong suppression of the ionization probability at small *R*. As a consequence the Franck-Condon distribution is shifted to larger *R* which reduces the number of more energetic fragments. Such an effect has been demonstrated in a recent joint experimental and theoretical work (Urbain *et al*

2004) for the population of vibrational states of H_2^+ in strong-field single ionization of H_2.

The question remains whether all dissociation products are restricted to the low-energy region. Figure 8 displays the proton energy spectra corresponding to the coincidence diagram in Figure 5b and curve 1 in Figure 3c. The dashed line shows the energy distribution for the events where two protons are detected in coincidence and momentum conservation is fulfilled. This makes the separation of double ionization and dissociation events more reliable. The spectra are scaled in order to match the number of single proton events in the CREI region. Regions of the spectrum where random coincidences cannot be excluded are marked by shaded areas. We find a significant deficit of coincident events around 3 to 6 eV, i.e. in the region of SDI. This indicates indirectly a contribution of dissociation since neutral fragments are not detected. The origin of this energetic dissociation fragments remains unclear. One possible contribution can be given by the RESI mechanism for NSDI. In its second step the electron in the recollision-induced excited state is field-ionized. If the laser pulse duration is short enough even at high peak intensities some population in excited states may survive. Since all corresponding potential curves are repulsive, the electronically excited molecule will dissociate. Figure 1 shows that e.g. recollision population of the first excited state $2p\sigma_u$ will lead to a total KER of 5 to 12 eV (i.e. 3 to 6 eV per proton) which is in good accordance with our experimental findings. Similar values are expected for the $2p\pi_u$ state. There is an ongoing debate whether dissociation or CE is the dominating channel in the “molecular clock” scheme. Niikura *et al* 2003a,b attributed the main feature in the fragment spectrum around 6 eV to the dissociation of recollision-excited molecular ions. However, their non-coincident experiment could not distinguish reliably between dissociation and CE.

More recently Tong *et al* 2003 demonstrated that both channels contribute and discussed in detail the noncoincident and coincident (Alnaser *et al* 2003) spectra. For the dissociation fragments a KER per particle of 2 to 7 eV is calculated which is in reasonable agreement with our results. However, it seems unlikely that in our case recollision-induced dissociation is the dominant source of the high-energy dissociated protons since we do not restrict the solid angle in order to select the recollision contribution, as was done in the experiment of Alnaser *et al* (2003).

5. Conclusions and outlook

We have studied the dynamics of molecular hydrogen fragmentation by intense laser pulses of different durations. For 25 fs pulses we observed the spectra well-known from previous studies, with 1ω and 2ω dissociation peaks, a broad CREI structure and high-energy tail due to recollision-induced Coulomb explosion. When the pulse width is reduced, the two-peak dissociation structure in the proton kinetic energy spectra is smeared out, and for 7fs becomes closer to the Franck-Condon distribution. Coulomb explosion (CREI) contribution is suppressed, and “atomic-like” sequential double ionization which results in the production of the protons with higher kinetic energies starts to be distinguishable. The intensity dependence of this SDI is in a good qualitative agreement with the recent theoretical results (Tong and Lin 2004). Coincident measurements revealed the existence of a low-energy Coulomb explosion peak which for non-coincident data is hidden in the dissociation part. Experiments with different pulse shapes showed that this structure is most likely due to delayed ionization caused by the post pulses at large internuclear distances. This low-energy structure, as well as residual CREI contribution can be enhanced (see curve 1 in

Figure 3c, Figure 5b and Figure8), if 7 fs pulses with higher pre and post pulses are used.

There are several questions that remain open. The low-energy CE peak seems to be well-localized. An interesting point is whether two double ionization peaks 1n Figure 8 (at ~ 1.5 and 2.5 eV) reflect two maxima in the R-dependence of the probability of enhanced ionization, that were predicted theoretically (see, e.g. Zuo and Bandrauk 1995) but never observed experimentally. To answer this question, pump-probe experiments with few-cycle pulses are planned. Another problem concerns the observed deficit of coincidence events for proton kinetic energies of 3-6 eV. To clarify this point, more detailed coincident measurements with "clean" 7 fs pulses together with reliable time-dependent description of the fragmentation process are required. And, of course more information on the dynamics of different fragmentation channels can be obtained from the coincident electron spectra. First results for 30 fs were reported earlier (Rottke *et al* 2002), and the experiments with few-cycle pulses are under way.

The authors are grateful to H. Rottke and A. Voitkiv for valuable discussions.

References

Alnaser A S, Osipov T, Benis E P, Wech A, Shan B, Cocke C L, Tong X M and Lin C D 2003 *Phys. Rev. Lett.* **91** 163002

Bandrauk A D and Sink M L 1981 *J. Chem. Phys*. **74** 1110

Bandrauk A D and Shon M H 2002 *Phys Rev. A* **66** 031401

Bucksbaum P H, Zavriyev A, Muller H G and Schumacher D W 1990 *Phys. Rev. Lett*. **64** 1883

Chelkovski S, Conjusteau A, Zuo T and Bandrauk A 1996 *Phys. Rev. A* **54** 3235

Chelkovski S, Corkum P B and Bandrauk A 1999 *Phys. Rev. Lett.* **82** 3416

Dundas D, McCann J F, Parker J S and Taylor K T 2000 *J. Phys. B* **33** 3261

Feuerstein B, Moshammer R, Fischer D, Dorn A, Schröter C D, Deipenwisch J, Crespo Lopez-Urrutia J R, Höhr C, Neumayer P, Ullrich J, Rottke H, Trump C, Wittmann M, Korn G and Sandner W 2001 *Phys. Rev. Lett.* **87** 043003

Feuerstein B and Thumm U 2003 *Phys. Rev. A* **67** 043405

Frasinski L J, Posthumus J H, Plumridge J, Codling K, Taday P F and Langley A J 1999 *Phys. Rev. Lett.* **83** 3625

Gibson G N, Li M, Guo C and Neira J 1997 *Phys. Rev. Lett.* **79** 2022

Giusti-Suzor A, He X, Atabek O and Mies F H 1990 *Phys. Rev. Lett.* **64** 515

Giusti-Suzor A, Mies F H, DiMauro L f, Charron E and Yang B 1995 *J. Phys. B* **28** 309

Harumiya K, Kono H,Fujimura Y, Kawata I and Bandrauk A 2002 *Phys. Rev. A* **66** 043403

de Jesus V L B, Rudenko A, Feuerstein B, Zrost K, Schröter C D, Moshammer R and Ullrich J 2004a *J. J. Electron Spectrosc. Relat. Phenom.* (in press)

de Jesus V L B, Feuerstein B, Zrost K, Fischer D, Rudenko A, Afaneh F, Schröter C D, Moshammer R and Ullrich J 2004b *J. Phys. B* **37** L161

Niikura H, Légaré F, Hasbani R, Bandrauk A D, Ivanov M Y, Villeneuve D M and Corkum P B 2002 *Nature* **417** 917

Niikura H, Légaré F, Hasbani R, Ivanov M Y, Villeneuve D M and Corkum P B 2003 *Nature* **421** 826

Numico R, Keller A and Atabek O 1997 *Phys. Rev. A* **56** 772

Osipov T, Alnaser A S, Voss S, Prior M H, Weber T, Jagutzki O, Schmidt L, Schmidt-Bocking H, Dorner R, Landers A, Wells E, Shan B, Maharjan C, Ullrich B, Ranitovic P, Tong X M, Lin C D and Cocke C L 2004 *J Mod. Opt.* (in press)

Plummer M and McCann J F 1996 *J. Phys. B* **29** 4625

Posthumus J H, Plumridge J, Frasinski L J, Codling K, Divall E J, Langley A J and Taday P F 2000 *J. Phys. B* **33** L563

Posthumus J H 2004 *Rep. Prog. Phys.* **67** 623

Rottke H, Trump C, Wittmann M, Korn G, Sandner W, Moshammer R, Dorn A, Schröter C D, Fischer D, Crespo López-Urrutia J R, Neumayer P, Deipenwisch J, Höhr C, Feuerstein B, and Ullrich J 2002 *Phys. Rev. Lett*. **89** 013001

Saenz A 2002a *Phys. Rev. A* **66** 063407

Saenz A 2002b *Phys. Rev. A* **66** 063408

Sakai H, Larsen J J, Wendt-Larsen I, Olesen J, Corkum P B and Stapelfeldt H 2003 *Phys. Rev. A* **67** 063404

Sändig K, Figger H and Hänsch T W 2000 *Phys. Rev. Lett*. **85** 4876

Shellhammer C, Schyja V, Hielscher A and Helm H 2000 *Laser and Particle Beams* **18** 443

Shirley J H 1965 *Phys. Rev*. **138** B979

Staudte A, Cocke C L, Prior M H, Belkacem A, Ray C, Chong H W, Glover T E, Schoenlein R W and Saalmann U 2002 *Phys. Rev. A* **65** 020703

Thomson M R, Thomas M K, Taday P F, J, Posthumus J H, Langley A, Frasinski L J and Codling K J 1997 *J. Phys. B* **30** 5755

Tong X M, Zhao Z X and Lin C D 2003 *Phys. Rev. A* **68** 043412

Tong X M and Lin C D 2004 *Phys. Rev. A* **70** 023406

Ullrich J, Moshammer R, Dorn A, Dörner R, Schmidt L Ph H and Schmidt-Böcking H 2003 *Rep. Prog. Phys*. **66** 1463

Urbain X, Fabre B, Staicu-Casagrande E M, de Ruette N, Andrianarijaona V M, Jureta J, Posthumus J H, Saenz A, Baldit E and Cornaggia C 2004 *Phys. Rev. Lett*. **92** 163004

Walsh T D G, Ilkow F A and Chin S I 1997 *J. Phys. B* **30** 2167

Walsh T D G, Ilkow F A, Chin S I, Châteauneuf F, Nguyen-Dang T T, Chelkovski S, Bandrauk A and Atabek O 1998 *Phys. Rev. A* **58** 3922

Weber Th, Weckenbrock M, Staudte A, Spielberger L, Jagutzki O, Mergel V, Afaneh F, Urbasch G, Vollmer M, Giessen H and Dörner R 2000 *J. Phys. B* **33** L127

Yu H, Zuo T and Bandrauk A 1996 *Phys. Rev. A* **54** 3290

Zavriyev A, Bucksbaum P H, Squier J and Saline F 1993 *Phys. Rev. Lett*. **70** 1077

Zuo T and Bandrauk A 1995 *Phys. Rev. A* **52** R2511

Figure legends:

Figure 1. Potential curves of two lowest electronic states of H_2^+ dressed with n (n = 1,2,3) photons. Arrows indicate different fragmentation pathways.

Figure 2. H_2 fragmentation spectra with 25 fs pulses at 0.2 PW/cm^2.
(a) Typical time-of–flight ion spectra. The dashed vertical line indicates time-of-flight of the protons with zero momentum along the field polarization direction. (b) Solid line: corresponding proton energy spectrum for the "forward" protons (see text). Dashed line: the data obtained with circularly polarized light. The curve is normalized to fit the 2ω peak for linear polarization. In circular case the intensity was 2 times lower.

Figure 3. Evolution of the proton time-of-flight spectra with the pulse duration.

(a) 25 fs pulses with the intensities of 0.2, 0.3 and 0.5 PW/cm^2 for the lower, middle and upper curve, respectively. The curves are separated in vertical direction for visual convenience. (b) 10 fs, 0.5 PW/cm^2. (c) 7 fs, 0.8 PW/cm^2. Curves 1 and 2 were obtained with the pulses of different shape (see text and Figure 4).

Figure 4. Characteristics of two laser pulses corresponding to the results of Figure 3c.
(a), (d) Measured frequency spectra. (b), (e): Fourier limit for the intensity profile.
(c), (f) Measured 2nd order autocorrelation. Panels (a)-(c) and (d)-(f) correspond to the curves 1 and 2 in Figure 3c, respectively.

Figure 5. Coincidence diagram of the proton longitudinal momenta.
The momentum of the protons detected on the detector as a first hit ($P_1^{\parallel}$) is plotted versus the momentum of the second one ($P_2^{\parallel}$). The momentum distribution is recalculated from the ion time-of-flight and thus contains the contribution of H_2^+ ions

(a peak above 30 a.u.) which does not reflect their momenta. The real coincidences lay near the diagonal $P_1^{\parallel} = - P_2^{\parallel}$ due to momentum conservation.
(a) 25 fs, 0.5 PW/cm^2. (b) 7 fs, 0.8 PW/cm^2. The diagram corresponds to the curve 1 in Figure 3c and panels (a)-(c) in Figure 4. For discrete Coulomb explosion peaks the estimated values of the internuclear distances R are indicated.

Figure 6. Proton kinetic energy distributions obtained with 7 fs laser pulse.
The curves are separated in vertical direction for visual convenience. The intensities from up to down: 2.0 PW/cm^2, 1.4 PW/cm^2, 0.8 PW/cm^2, 0.5 PW/cm^2, 0.3 PW/cm^2, 0.2 PW/cm^2. The data were obtained with the "clean" pulses (the curve for 0.8 PW/cm^2 corresponds to the curve 2 in Figure 3c and panels (d)-(f) in Figure 4). Vertical arrows indicate positions of SDI maxima. Dashed lines show a Franck-Condon distribution (see text).

Figure 7. Sum longitudinal momentum of two coincident protons created by sequential (a), (c) and non-sequential (b), (d) double ionization of H_2 at 0.5 PW/cm^2. (a), (b): 25fs. (c), (d): 7fs.

Figure 8. Kinetic energy spectra of coincident and non-coincident protons.
The set of data is the same as for the Figure 5b and curve 1 in Figure 3c. Solid line: all events. Dashed line: events, detected in coincidence. Shaded areas mark the regions, where false coincidences cannot be excluded.

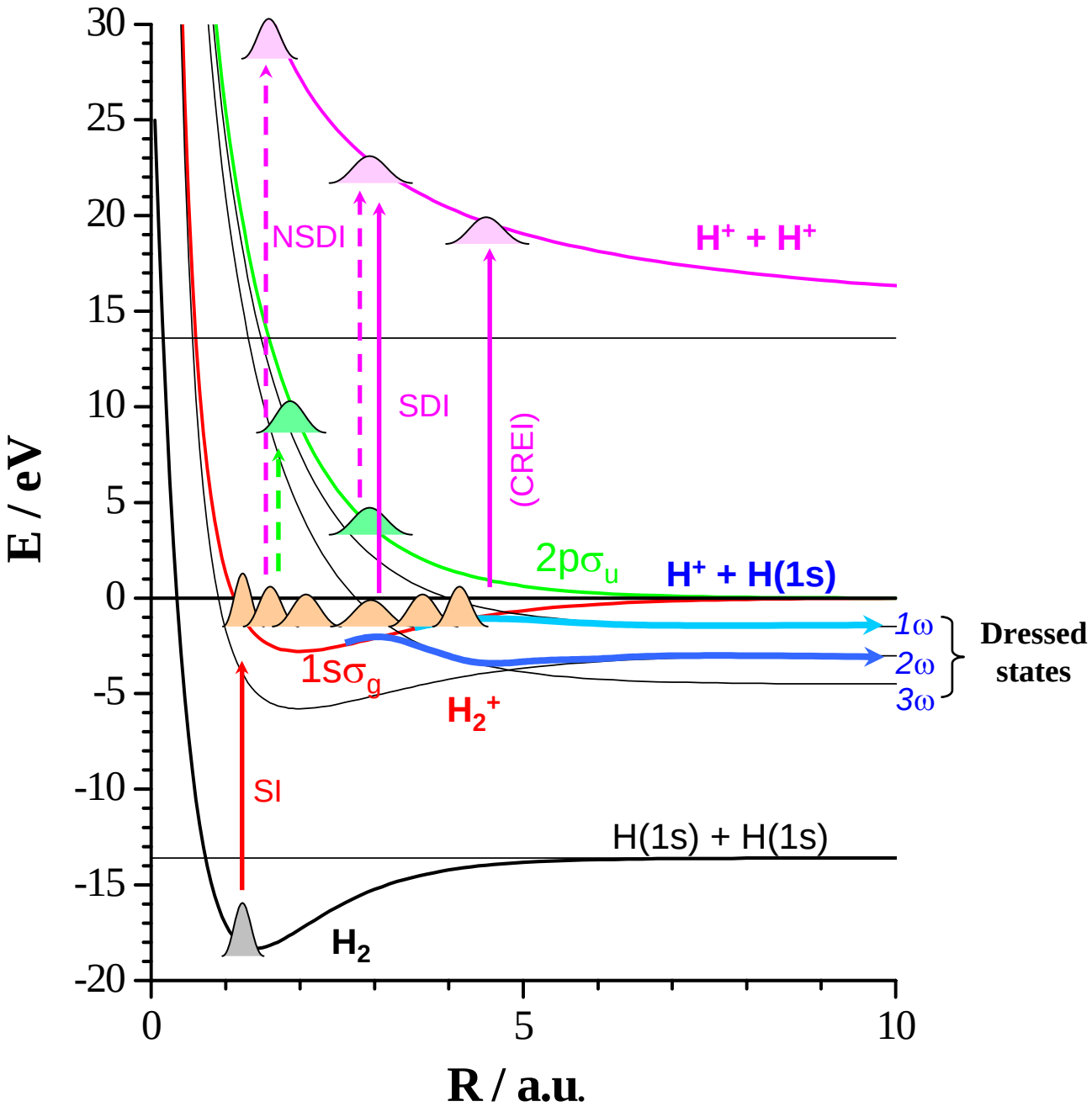

Figure 1 (color online)

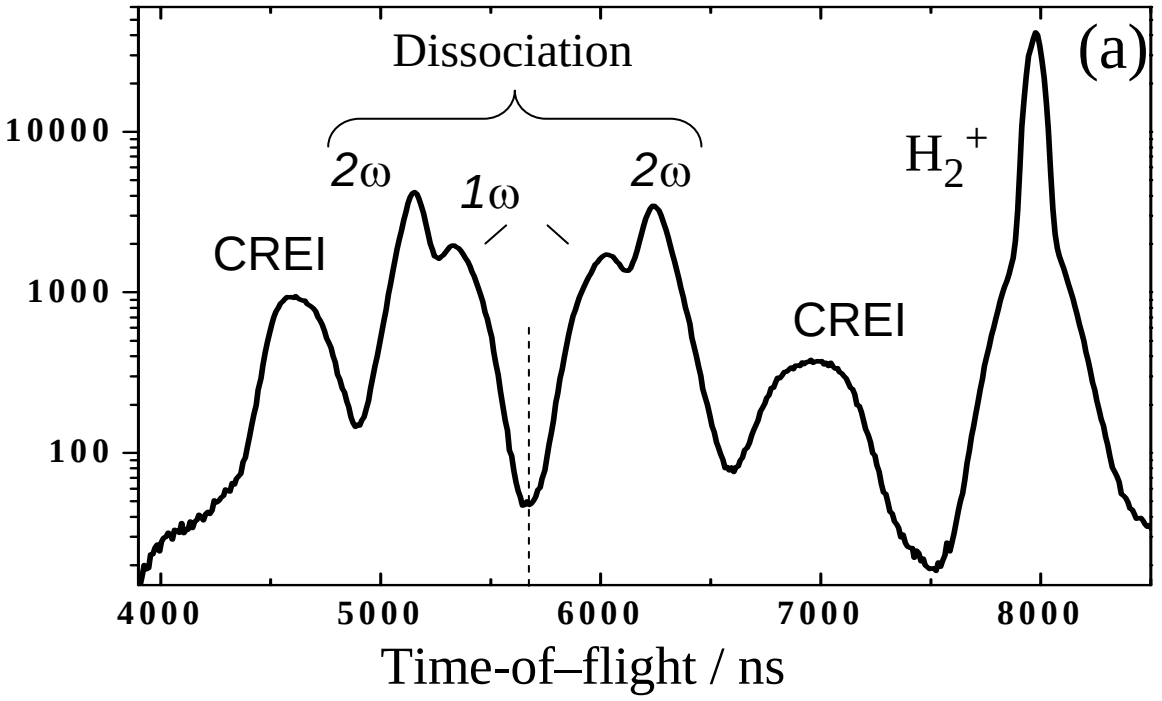
(a)
Dissociation
2ω
1ω
2ω
CREI
CREI
H2+
10000
1000
100
4000
5000
6000
7000
8000
Time-of–flight / ns

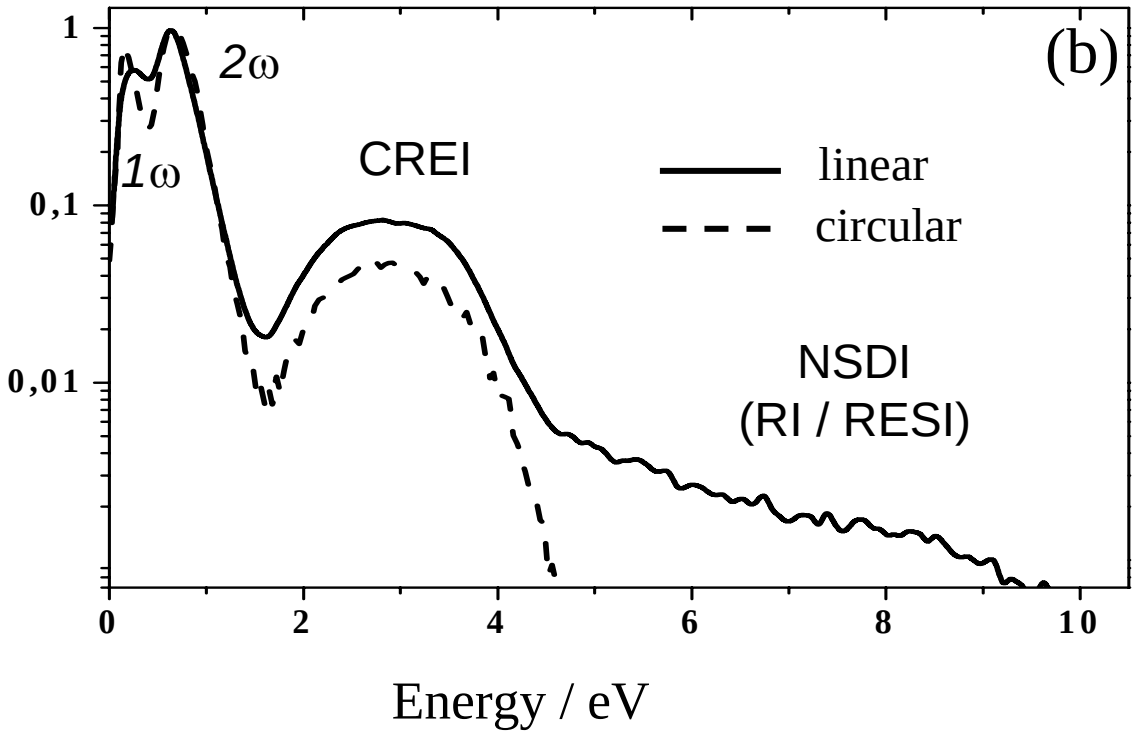
(b)
2ω
1ω
CREI
linear
circular
NSDI
(RI / RESI)
1
0,1
0,01
0
2
4
6
8
10
Energy / eV

Figure 2

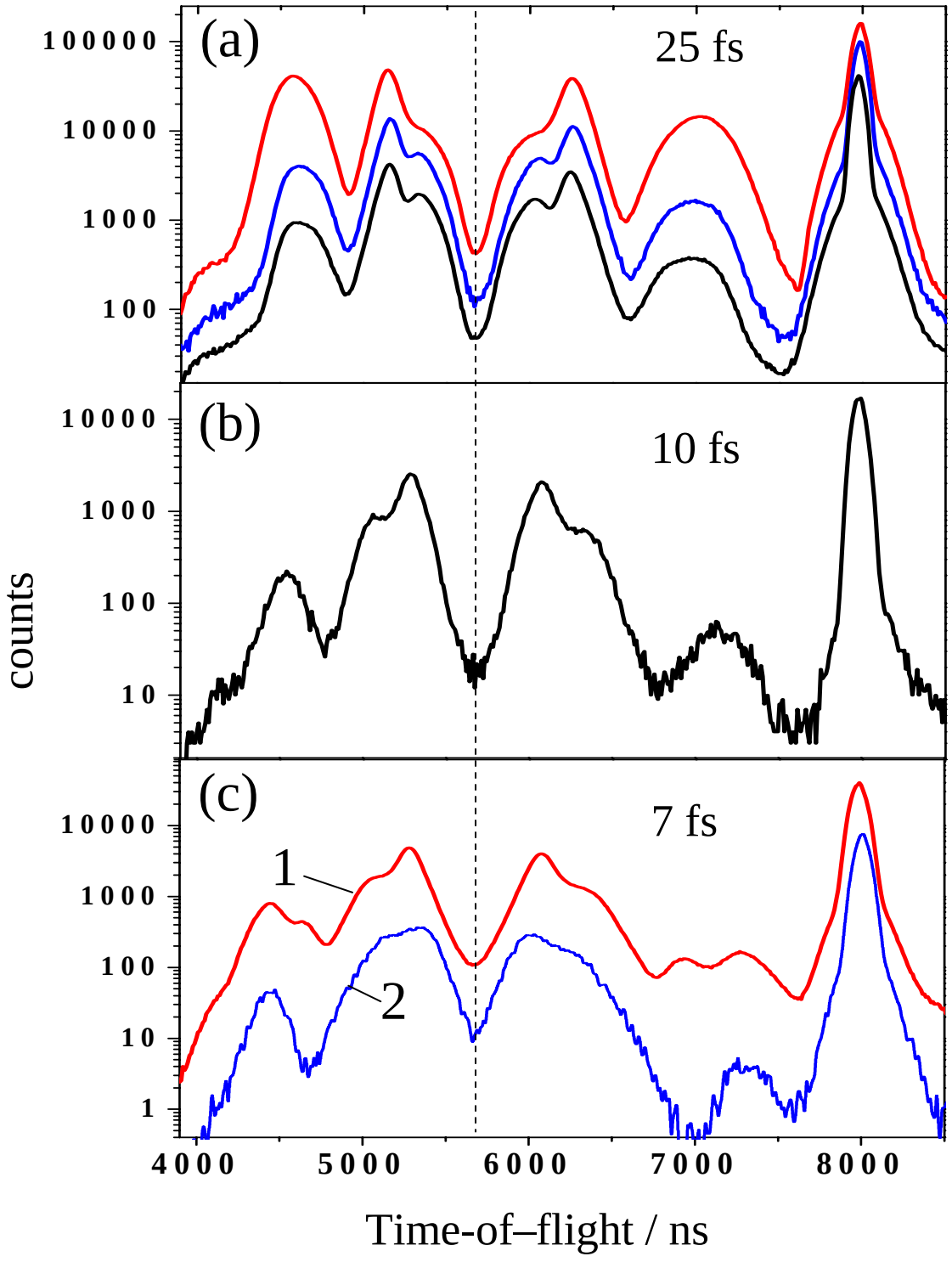

Figure 3 (color online)

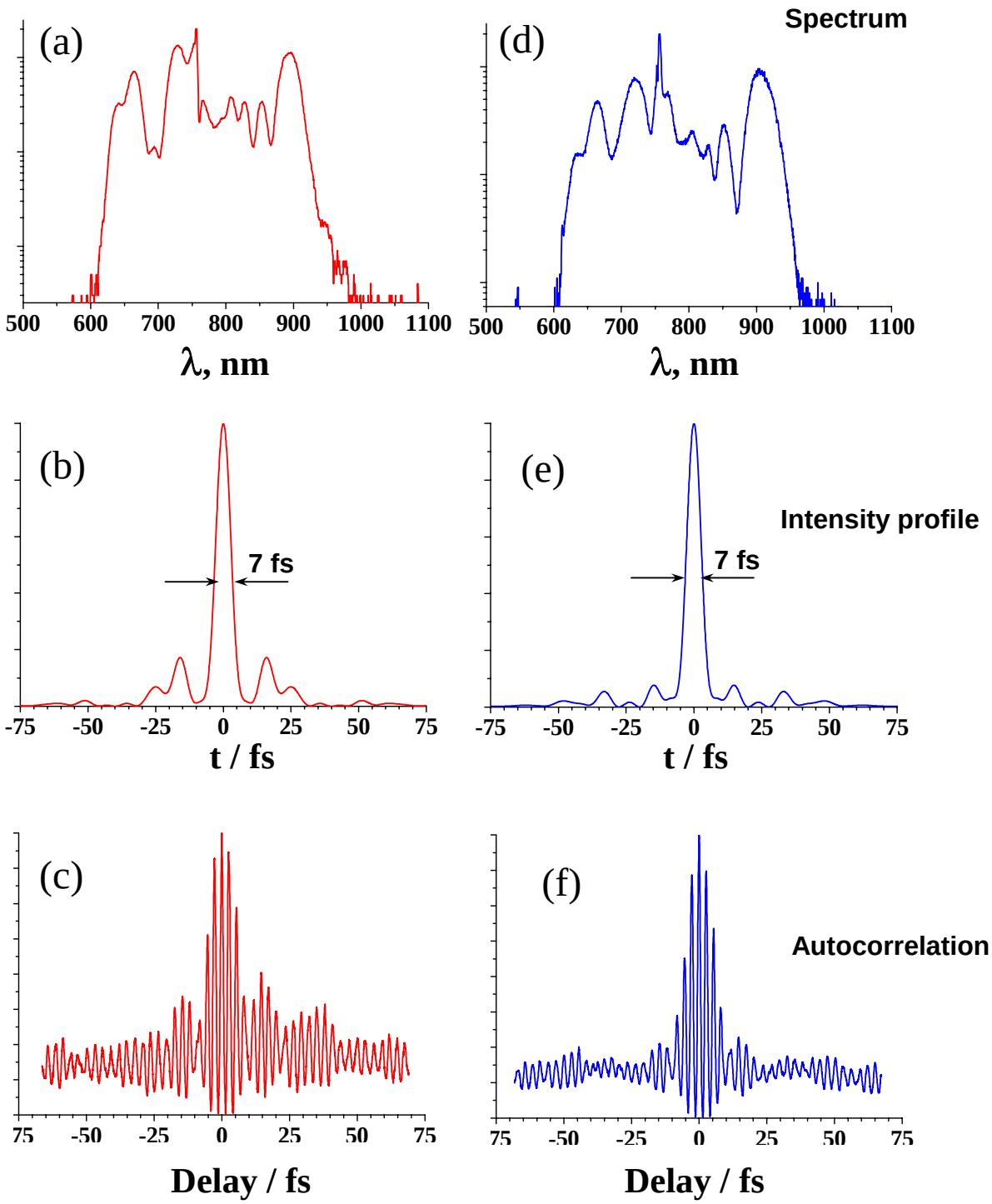

Figure 4 (color online)

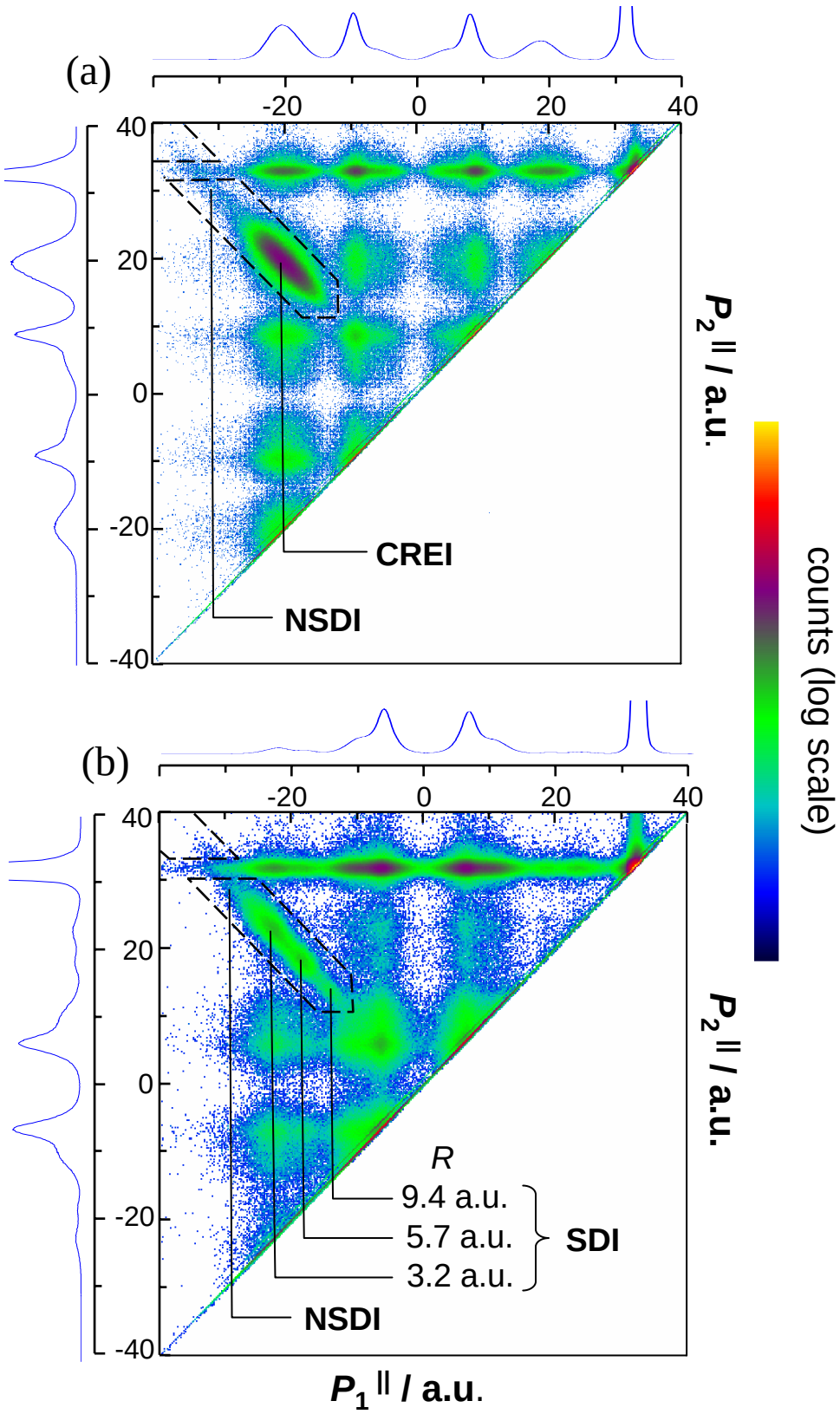

Figure 5 (color online)

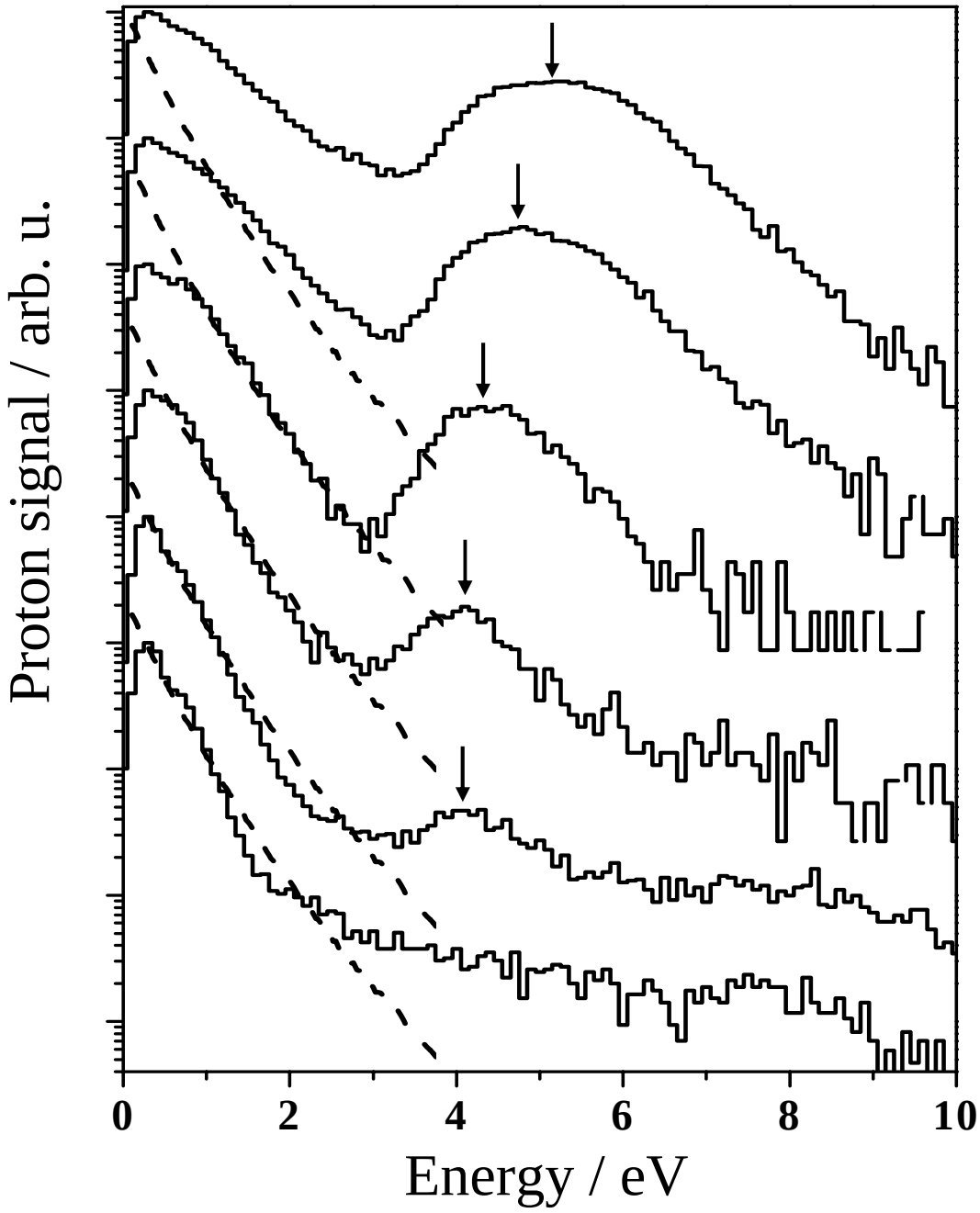

Figure 6

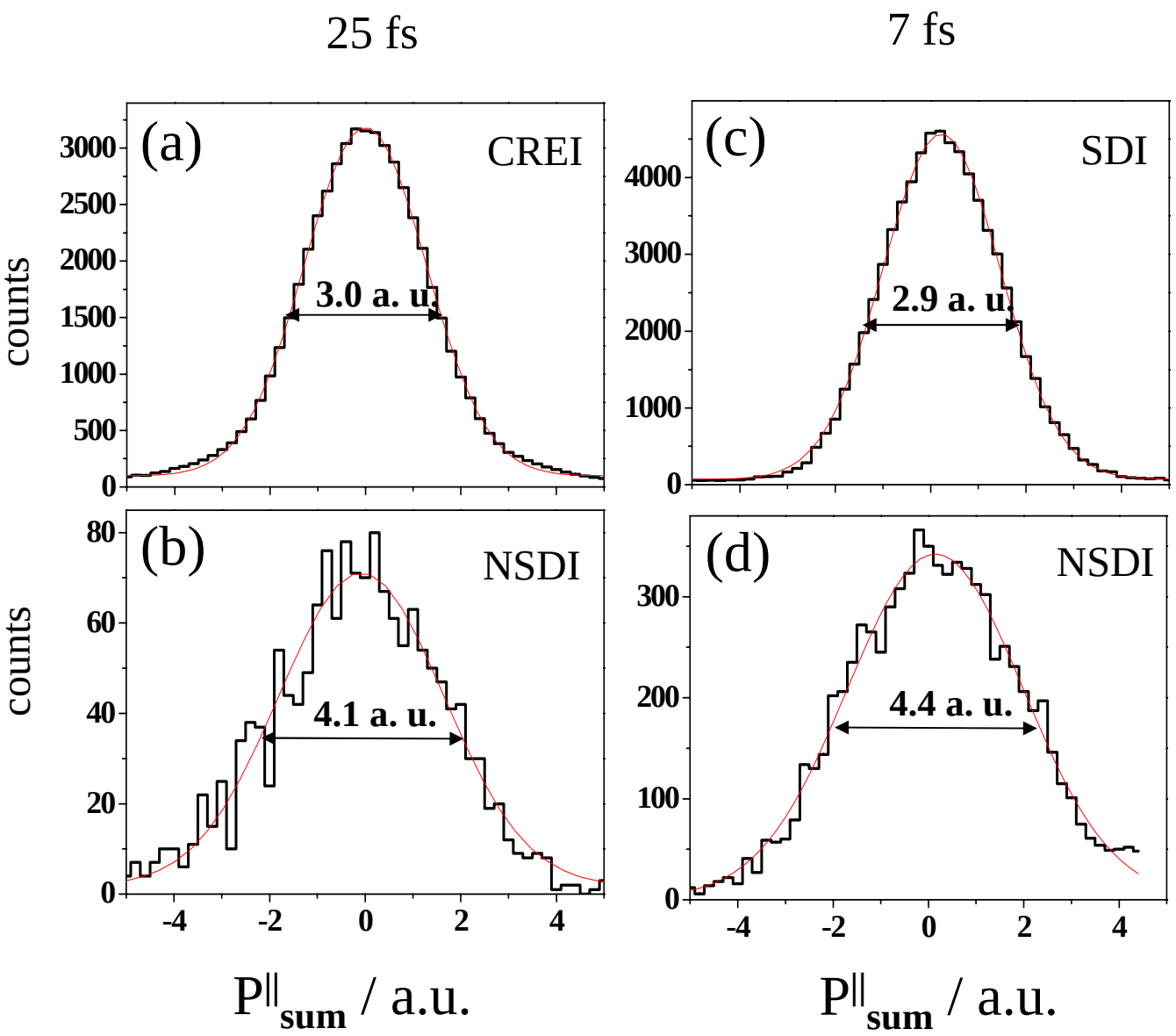
25 fs
7 fs
(a)
CREI
3.0 a. u.
(c)
SDI
2.9 a. u.
(b)
NSDI
4.1 a. u.
(d)
NSDI
4.4 a. u.
counts
counts
P||sum / a.u.
P||sum / a.u.

Figure 7

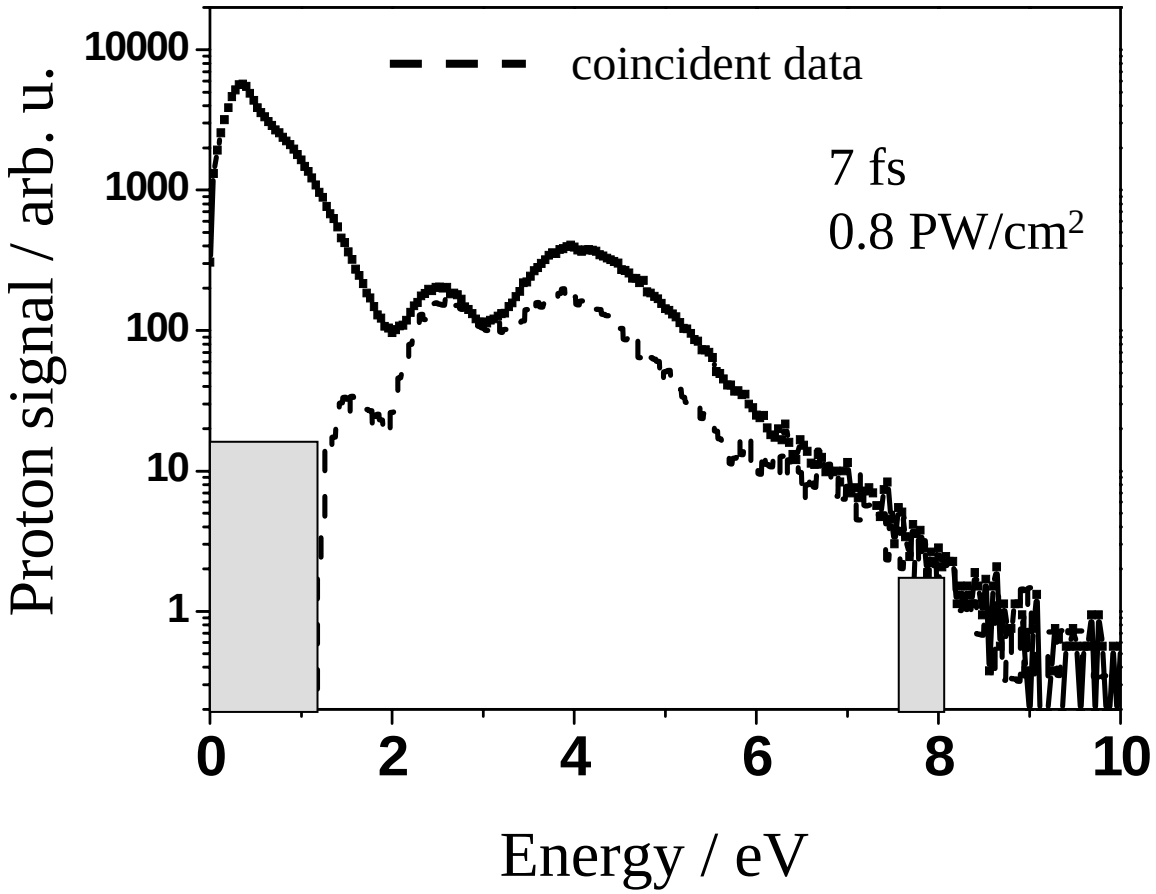
coincident data
7 fs
0.8 PW/cm2
Proton signal / arb. u.
10000
1000
100
10
1
0
2
4
6
8
10
Energy / eV

Figure 8